Elliptic-blending second-moment turbulence closure with using an algebraic anisotropic dissipation rate tensor model

Jong Keun Shin

Department of Automotive Engineering, Hanzhong University,
119, Jiheung-dong, Donghae, Kangwondo 240-713, Korea
jkshin@hanzhong.ac.kr

Jeong Soo An, Young Don Choi

Department of Mechanical Engineering, Korea University,
1, Anam-dong, Sungbuk-ku, Seoul 136-701, Korea
anjsoo@korea.ac.kr, ydchoi@korea.ac.kr

ABSTRACT

This study describes the amendment of an algebraic anisotropic dissipation rate model (ADRM) and its application to various turbulent flows to test the model's performance. Modeling anisotropies for the turbulence dissipation rate is considered by an analysis of the exact transport equation for the dissipation rate tensor. The second-moment closure, which is based on the explicit amended ADRM, is proposed and it is closely linked to the elliptic-blending model that is used for the prediction of Reynolds stresses.

The prediction results are directly compared to the DNS and the LES to assess the performance of the new model predictions and to show their reasonable agreement with the DNS and LES data for all the flow fields that were analyzed for the present study.

1. INTRODUCTION

Speziale and Gatski[1] (hereinafter, SG) suggested a new algebraic anisotropic dissipation rate model (ADRM), which was invoked by a local equilibrium hypothesis. This ADRM led to a scalar dissipation rate equation and an algebraic expression for the anisotropy of the dissipation rate tensor. Both the anisotropy of the dissipation rate tensor and the coefficient in the dissipation rate equation were found to be nonlinear functions of the mean velocity gradient. This distinguished it from many previously proposed scalar dissipation rate equations.

Although the SG-ADRM was reasonably successful for homogeneous turbulent flows, we think that a margin for improvement has remained in that model for near-wall turbulence. That is, we aim to extend the ADRM to a full second-moment treatment considering a near-wall turbulence prediction. Therefore, the ADRM that is only constructed in the anisotropy of dissipation, d_{ij}, is amended with the anisotropic tensor of the Reynolds stress, b_{ij}, in order for it to apply to the inhomogeneous turbulent flow in this study. An implicit system of algebraic equations for the amended ADRM will then be obtained after the same type of local equilibrium hypothesis is invoked as that which gives rise to the algebraic stress description of the gas-solid turbulent flows that were suggested by Mashayek and Taulbee[2]. Since the implicit form of this equation makes it inconvenient to perform actual computations, we converted the present, amended ADRM into an explicit equation, which was generated with using the Cayley-Hamilton theorem.

Modeling the Reynolds stress transport equations was closely coupled with the amended ADRM and it was accomplished with using the elliptic-blending equation, which was suggested by Thielen et al.[3]. It was based on the blending of near-wall and far-from-wall forms of the pressure scrambling correlation. A notable feature of this approach is that the non-local character is preserved by the elliptic operators such as the elliptic-blending equation, and the formulations can be integrated down to the wall.

The present second-moment model that uses the amended ADRM has been integrated numerically for several different inhomogeneous test cases and the results were compared with DNS and LES to assess the performance of the proposed model.

2. MATHEMATICAL MODELS

2.1 The amended algebraic anisotropic dissipation rate tensor model

According to the SG[1], the exact transport equation for the dissipation rate tensor, ϵ_{ij}, for homogeneous turbulence takes the forms:

$$\dot{\epsilon}_{ij} = -\left(\epsilon_{ik}\frac{\partial U_j}{\partial x_k} + \epsilon_{jk}\frac{\partial U_j}{\partial x_k}\right) + P_{ij}^{2\epsilon} + \Phi_{ij}^{\epsilon} + \Gamma_{ij}^{\epsilon} \qquad (1)$$

where

$$P_{ij}^{2\epsilon} = -2f_{ijkl}\frac{\partial U_k}{\partial x_l} \qquad (2)$$

$$\Phi_{ij}^{\epsilon} = 2(f_{ikjl} + f_{jkil})\frac{\partial U_k}{\partial x_l} + C_{\epsilon5}\frac{\epsilon}{k}\left(\epsilon_{ij} - \frac{2}{3}\epsilon\delta_{ij}\right) \qquad (3)$$

$$\Gamma_{ij}^{\epsilon} = \frac{2}{3}\left(C_{\epsilon1}\frac{\epsilon}{k}P - C_{\epsilon2}\frac{\epsilon^2}{k}\right)\delta_{ij} \qquad (4)$$

The coefficients of the mean velocity gradient of $P_{ij}^{2\epsilon}$ and the rapid term of Φ_{ij}^{ϵ} are written in terms of a 4th-order tensor $f_{ijkl} = 2\nu\overline{(\partial u_k/\partial x_i)(\partial u_l/\partial x_j)}$. In order to model the $P_{ij}^{2\epsilon}$ and the rapid term of Φ_{ij}^{ϵ}, we use a new 4th-order tensor that is composed from both the correlation of the dissipation rate anisotropy tensor, d_{ij}, and the Reynolds stress anisotropy tensor, b_{ij}. That is , d_{ij} is considered for the redistribution effect and b_{ij} is used for the production rate effect. The most general linear model for both d_{ij} and b_{ij} is obtained from

$$\frac{f_{ijkl}}{\epsilon} = \alpha_1\delta_{ij}\delta_{kl} + \alpha_2(\delta_{ik}\delta_{jl} + \delta_{il}\delta_{jk}) \qquad (5)$$
$$+ \alpha_3\delta_{ij}d_{kl} + \alpha_4\delta_{kl}d_{ij}$$
$$+ \alpha_5(\delta_{ik}d_{jl} + \delta_{jk}d_{il} + \delta_{il}d_{jk} + \delta_{jl}d_{ik})$$
$$+ \alpha_3\delta_{ij}b_{kl} + \alpha_4\delta_{kl}b_{ij}$$
$$+ \alpha_5(\delta_{ik}b_{jl} + \delta_{jk}b_{il} + \delta_{il}b_{jk} + \delta_{jl}b_{ik})$$

In equation (5), d_{ij} and b_{ij} are respectively defined as:

$$d_{ij} = \frac{\epsilon_{ij}}{2\epsilon} - \frac{1}{3}\delta_{ij}, \quad b_{ij} = \frac{\overline{u_iu_j}}{2k} - \frac{1}{3}\delta_{ij} \qquad (6)$$

From the consideration of a homogeneous turbulent flow in the equilibrium state, a linear algebraic equation is obtained as follows:

$$\frac{\epsilon}{k}\left(\frac{P}{\epsilon} - 1\right)d_{ij} = -d_{ik}\frac{\partial U_j}{\partial x_k} - d_{jk}\frac{\partial U_i}{\partial x_k} - \frac{2}{3}S_{ij} \qquad (7)$$
$$+ \frac{1}{2\epsilon}\left[2(f_{ikjl} + f_{jkil} - f_{lkij})\frac{\partial U_k}{\partial x_l}\right] - C_{\epsilon5}\frac{\epsilon}{k}d_{ij}$$
$$+ \frac{1}{3}\left[(C_{\epsilon1} - 1)\frac{P}{k} - (C_{\epsilon2} - 1)\frac{\epsilon}{k}\right]\delta_{ij}$$

After applying the 4th-order tensor equation (5) through (7), and with using the symmetry, continuity, normalization and complementary constraints for the 4th-order tensor, the amended algebraic anisotropic dissipation rate tensor model(amended ADRM), d_{ij}, takes the form:

$$\frac{\epsilon}{k}\left(\frac{P}{\epsilon} - 1\right)d_{ij} = -d_{ik}\frac{\partial U_j}{\partial x_k} - d_{jk}\frac{\partial U_i}{\partial x_k} - C_{\epsilon5}\frac{\epsilon}{k}d_{ij} \qquad (8)$$
$$- \frac{2}{15}S_{ij} + \frac{2}{3}d_{lk}S_{kl}\delta_{ij}$$
$$+ \left(\frac{15}{11}\beta + \frac{10}{11}\right)\left(d_{ik}S_{jk} + d_{jk}S_{ik} - \frac{2}{3}d_{lk}S_{kl}\delta_{ij}\right)$$
$$- \left(\frac{7}{11}\beta - \frac{10}{11}\right)(d_{ik}W_{jk} + d_{jk}W_{ik})$$
$$+ \frac{15}{11}\gamma\left(b_{ik}S_{jk} + b_{jk}S_{ik} - \frac{2}{3}b_{lk}S_{kl}\delta_{ij}\right)$$
$$- \frac{7}{11}\gamma(b_{ik}W_{jk} + b_{jk}W_{ik})$$

where,

$$S_{ij} = \frac{1}{2}\left(\frac{\partial U_i}{\partial x_j} + \frac{\partial U_j}{\partial x_i}\right), \quad W_{ij} = \frac{1}{2}\left(\frac{\partial U_i}{\partial x_j} - \frac{\partial U_j}{\partial x_i}\right) \qquad (9)$$

S_{ij} and W_{ij} are the mean strain rate and the mean vorticity tensor, respectively. The last two terms of the RHS in equation (8), which are only related to the anisotropy of the Reynolds stress, b_{ij}, are added to the model of SG when the equation is compared to the original ADRM of SG.

Detailed expressions for the ADRM and their model coefficients can be found in SG[1].

Equation (8) contains three arbitrary coefficients, β, γ and $C_{\epsilon5}$. The coefficient, β, was determined to be 0.6 in SG, which was accomplished by using the DNS data for homogeneous shear flow from Rogers et al.[4]. However, in this study, we reconsider the coefficient, β, through the fully developed channel flow calculation and through the comparison with the DNS data of Moser et al.[5], which is maintained at 0.6 in homogeneous turbulence as in SG, and it can simultaneously reflect the inhomogeneous effect in the turbulent shear layer. Also, the coefficient γ is adjusted to be 0.15 from the computational procedures and $C_{\epsilon5}$ is assigned to be 5.8 according to SG.

For non-inertial references frames, the Coriolis term must be included in the RHS of equations (1) and (8). Furthermore, the mean vorticity tensor must be replaced with the absolute mean vorticity tensor as

$$W_{ij}^* = W_{ij} + e_{mji}\Omega_m. \qquad (10)$$

2.2 Explicit algebraic anisotropic dissipation rate tensor model

The amended algebraic dissipation rate tensor equation can be iteratively used for computation in the form presented above; however, the implicit form of this equation makes it inconvenient for actual computation. Thus, we will attempt to obtain an explicit form of the equation according to Mashayek and Taulbee[2]. To generate the explicit algebraic model, equation (8) is presented in tensor form as:

$$\underline{\underline{d}} = X_1\underline{\underline{q}} + X_2\left(\underline{\underline{d}}\,\underline{\underline{S}} + \underline{\underline{S}}\,\underline{\underline{d}} - \frac{2}{3}\{\underline{\underline{S}}\,\underline{\underline{d}}\}\underline{\underline{I_3}}\right) \quad (11)$$
$$+ X_3\left(\underline{\underline{d}}\,\underline{\underline{W}} - \underline{\underline{W}}\,\underline{\underline{d}}\right)$$

where, a double underline indicates a second-order tensor, $\underline{\underline{I_3}}$ is the three-dimensional identity tensor and $\underline{\underline{d}} = d_{ij}$. In equation (11), $\underline{\underline{q}}$ is a second-order tensor that represents the effect of the cross-correlation between d_{ij} and b_{ij}. The relations for the newly introduced coefficients and tensors are as follows:

$$X_1 = \frac{1}{\triangle\phi} \quad (12)$$

$$X_2 = \frac{15\beta - 1}{11\triangle\phi} \quad (13)$$

$$X_3 = \frac{7\beta + 1}{11\triangle\phi} \quad (14)$$

$$q_{ij} = -\frac{2}{15}S_{ij} + \frac{15}{11}\gamma\left(b_{ik}S_{jk} + b_{jk}S_{ik} - \frac{2}{3}b_{kl}S_{kl}\delta_{ij}\right) \quad (15)$$
$$-\frac{7}{11}\gamma\left(b_{ik}W_{jk} + b_{jk}W_{ik}\right)$$

where,

$$\triangle\phi = \frac{\epsilon}{k}\left(\frac{P}{\epsilon} - 1 + C_{\epsilon5}\right) \quad (16)$$

The solution for $\underline{\underline{d}}$ is obtained by the Cayley-Hamilton theorem. The procedure is analogous to that for SG-ADRM. The difference is due to the fact that the tensor, $\underline{\underline{d}}$, is a function of three tensors ($\underline{\underline{S}}$, $\underline{\underline{W}}$ and $\underline{\underline{q}}$) here, in contrast to the case of SG, where $\underline{\underline{d}}$ is only a function of two tensors ($\underline{\underline{S}}$ and $\underline{\underline{W}}$). As a result, a new integrity basis and an irreducible matrix polynomial must be specified. In this study, we thoroughly used the Mashayek and Taulbee[2] method, which was introduced for deriving the explicit algebraic models for the gas-solid turbulent flows.

From the Mashayek and Taulbee expression, the tensor, $\underline{\underline{d}}$, can be expressed as a finite set of polynomials:

$$\underline{\underline{d}} = \sum_{\lambda}G^{\lambda}\underline{\underline{T}}^{\lambda} \quad (17)$$

where only the finite values, $\lambda = 1,2,3,4,5$, need to be considered, and where the $\underline{\underline{T}}^{\lambda}$s are the matrix polynomial functions of $\underline{\underline{S}}$, $\underline{\underline{W}}$, $\underline{\underline{q}}$, $\underline{\underline{I_2}}$ and $\underline{\underline{I_3}}$:

$$\underline{\underline{T}}^1 = \frac{1}{3}\underline{\underline{I_3}} - \frac{1}{2}\underline{\underline{I_2}}, \quad \underline{\underline{T}}^2 = \underline{\underline{S}}, \quad \underline{\underline{T}}^3 = \underline{\underline{S}}\,\underline{\underline{W}} - \underline{\underline{W}}\,\underline{\underline{S}},$$
$$\underline{\underline{T}}^4 = \underline{\underline{q}}, \quad \underline{\underline{T}}^5 = \underline{\underline{q}}\,\underline{\underline{W}} - \underline{\underline{W}}\,\underline{\underline{q}}, \quad (18)$$

The G^{λ} coefficients of the matrix polynomials are functions of the following invariants:

$$\eta_1 = \{\underline{\underline{S}}^2\}, \ \eta_2 = \{\underline{\underline{W}}^2\}, \ \eta_3 = \{\underline{\underline{S}}\,\underline{\underline{q}}\},$$
$$\eta_4 = \{\underline{\underline{S}}\,\underline{\underline{W}}\,\underline{\underline{q}}\} + \{\underline{\underline{W}}\,\underline{\underline{q}}\,\underline{\underline{S}}\} \quad (19)$$

The final step is to determine the G^{λ} coefficients in terms of the invariants, η_l, for $l = 1,2,3,4$. According to the Mashayek & Taulbee procedure, these G^{λ} coefficients are obtained as:

$$G^1 = \frac{-6X_1X_2X_3\eta_4 + 6X_1X_2\eta_3}{2X_2^2\eta_1 + 6X_3^2\eta_2 - 3} \quad (20a)$$

$$G^2 = \frac{2X_1X_2^2X_3\eta_4 - 2X_1X_2^2\eta_3}{\left(1 - 2X_3^2\eta_2\right)\left(2X_2^2\eta_1 + 6X_3^2\eta_2 - 3\right)} \quad (20b)$$

$$G^3 = \frac{2X_1X_2^2X_3^2\eta_4 - 2X_1X_2^2X_3\eta_3}{\left(1 - 2X_3^2\eta_2\right)\left(2X_2^2\eta_1 + 6X_3^2\eta_2 - 3\right)} \quad (20c)$$

$$G^4 = \frac{X_1}{1 - 2X_3^2\eta_2} \quad (20d)$$

$$G^5 = \frac{X_1X_3}{1 - 2X_3^2\eta_2} \quad (20e)$$

Therefore, we can see that the explicit solution for the dissipation rate anisotropy tensor, d_{ij}, is given by equation (17), and then ϵ_{ij} for homogenous turbulence can be obtained from equation (6), which is used in the Reynolds stress transport equation closure.

2.3 Elliptic-blending model for the turbulence stress tensor

We will employ the elliptic-blending second-moment closure that is suggested by Thielen et al.[3] in order to extend the dissipation rate anisotropy tensor, d_{ij}, which is obtained by considering homogeneous turbulence, to inhomogeneous turbulent flows. The model transport equations for the turbulent stress tensor are given as follows:

$$\frac{D\overline{u_iu_j}}{Dt} = \frac{\partial}{\partial x_k}\left(\left(\nu\delta_{kl} + C_s\overline{u_ku_l}T\right)\frac{\partial\overline{u_iu_j}}{\partial x_l}\right) \quad (21)$$
$$+ P_{ij} + \Phi_{ij}^* - \epsilon_{ij}$$

To impose a limiting wall behavior of the fluctuating quantities of the Reynolds stresses, Thielen et al. proposed the elliptic-blending method, which blends the "homogeneous" (away-from the wall) and near-wall models of Φ_{ij}^* and ϵ_{ij} as follows:

$$\Phi_{ij}^* = \left(1 - \psi^2\right)\Phi_{ij}^w + \psi^2\Phi_{ij}^h \quad (22)$$

$$\epsilon_{ij} = \left(1 - \psi^2\right)\frac{\overline{u_iu_j}}{k}\epsilon + \psi^2\epsilon_{ij}^h \quad (23)$$

In equation (23), the homogeneous part, ϵ_{ij}^h, is originally allocated to the isotropic model $(2\delta_{ij}/3)\epsilon$ by Thielen et al.[3]. However, we used the amended ADRM, which is ultimately obtained from equation (17), in order to consider the non-isotropic effect in the following form.

$$\epsilon_{ij}^h = 2\epsilon\left(d_{ij} + \frac{1}{3}\delta_{ij}\right) \tag{24}$$

Detailed expressions for the elliptic-blending model (EBM) and their model coefficients can be found in Thielen et al.[3].

The model transport equation for the energy dissipation rate is given in the expression of SG[1] for homogeneous turbulence and it can be extended to inhomogeneous turbulent flows with the addition of viscous and turbulent diffusion terms as follows:

$$\frac{D\epsilon}{Dt} = \frac{\partial}{\partial x_k}\left(\left(\nu\delta_{kl} + C_\epsilon\overline{u_ku_l}T\right)\frac{\partial\epsilon}{\partial x_l}\right) + \frac{C_{\epsilon 1}P - C_{\epsilon 2}\epsilon}{T} \quad (25)$$
$$- \left(\frac{21}{11}\beta + \frac{14}{11}\right)\epsilon d_{lk}S_{kl} - \left(\frac{21}{11}\gamma\right)\epsilon b_{lk}S_{kl}$$

In equation (25), the last two terms of the RHS are induced from the contraction of the dissipation rate tensor transport equation (1) for homogeneous turbulence. It is noted that the dissipation rate equation (25) differs from that suggested by Thielen et al.[3].

In the above equations, the turbulent time scale, T, and length scale, L, are bounded by Kolmogorov scales as follows (Durbin[6]):

$$T = \max\left(\frac{k}{\epsilon}, C_T\left(\frac{\nu}{\epsilon}\right)^{1/2}\right), \ L = C_L\max\left(\frac{k^{3/2}}{\epsilon}, C_\eta\frac{\nu^{3/4}}{\epsilon^{1/4}}\right) \tag{26}$$

The present elliptic-blending second-moment closure based on the amended ADRM adopts the coefficients of Table 1 from the calibration procedure for the model coefficients.

Table 1 The model coefficients for the present elliptic-blending second-moment closure.

C_s	C_ϵ	C_1	C_1^*	C_2	C_3	C_3^*	C_4
0.21	0.18	3.4	1.8	4.2	0.8	1.3	1.25
C_5	C_T	C_L	C_η	$C_{\epsilon 1}$	$C_{\epsilon 2}$	β
0.4	0.6	0.157	80.0	1.0	1.83	$\min(A^2, 0.6)$

3. NUMERICAL TREATMENT

For the assessment of the amended dissipation rate anisotropy tensor model, the Reynolds-averaged Navier Stokes equation (RANS) simulation, which uses the elliptic-blending second-moment closure, is performed for the fully developed rotating and non-rotating channel and square duct flows. The computations for channel and square duct flows are performed with a simple finite-volume solver, and the majority of the grids are in the low Reynolds number region ($y^+ \leq 70$), while the first grid is located at $y^+ \approx 0.45$. The Reynolds stresses, heat flux and mean velocities are all set to 0 at the wall, and the wall dissipation rate is $\epsilon = 2\nu(\partial\sqrt{k}/\partial y)^2$.

4. RESULT AND DISCUSSION

Reynolds stress profiles for fully developed non-rotating channel flows at $Re_\tau = 590$ are plotted in figure 1 and they are compared to the DNS of Moser et al.[5]. Figure 1 shows that the anisotropy is predicted well by the models, when it is compared to the DNS. The Reynolds stress profiles due to the present model are similar and reasonably close to the DNS. The profile of $\overline{u_3u_3}$ due to the present model is comparatively captured better than that of the Thielen-EBM, but the prediction due to the Thielen-EBM is slightly over-estimated in $y^+ \leq 100$.

Figure 2(a), which is related to the lower Rotation number $Ro_\tau = 0.05$, represents that the Thielen-EBM shows the over-estimated wall-normal stress profiles in the suction side of channel. The present model predictions for the rms velocities compare favorably with the DNS on both the pressure and suction sides, but some discrepancies are observed on the suction side. Although the prediction is limited to a relatively lower rotation rate, the accuracy of the prediction is still more
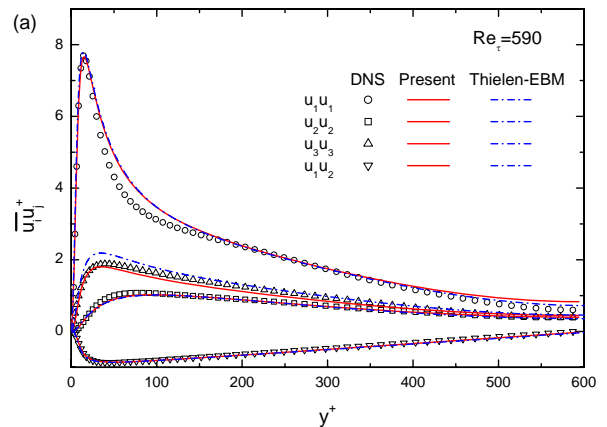
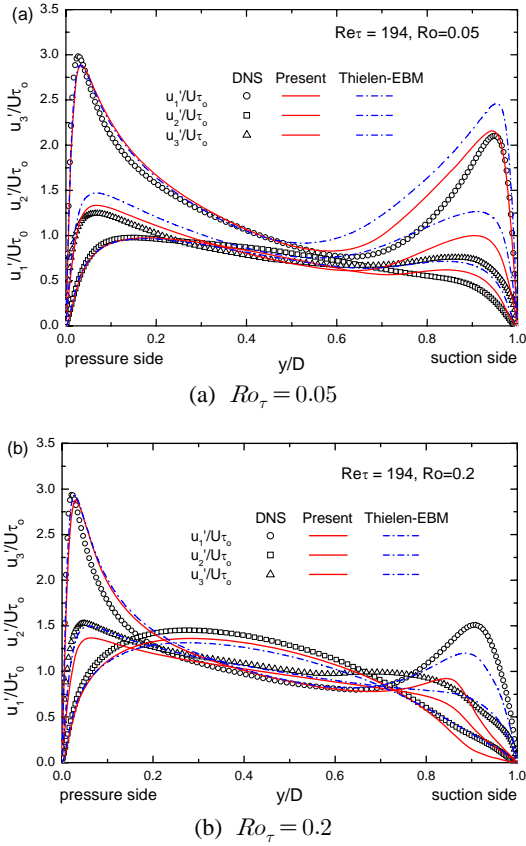**Figure 1** Distributions of Reynolds Stress in non-rotating channel at $Re_\tau = 590$.

(a) $Ro_\tau = 0.05$

(b) $Ro_\tau = 0.2$

Figure 2 Root mean square velocity fluctuations across the spanwise rotating channel for $Re_\tau = 194$.

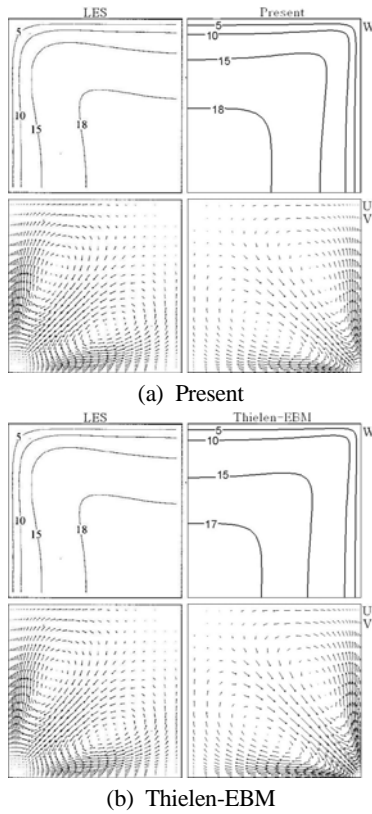(a) Present

(b) Thielen-EBM

Figure 3 Contours of streamwise mean velocity in a non-rotating square duct at $Re_\tau = 300$.

improved than when it is compared to the Thielen-EBM. However, figure 2(b), which is related to the rotation number $Ro_\tau = 0.2$, shows that the predictions due to the present model are under-estimated for the suction side when they are compared to the Thielen-EBM. When the rotation number is increased, the relaminarization on the suction side may occur more rapidly for the present model than for the Thielen-EBM. We think that the cause of the rapid relaminarization due to the present model is induced by the term involving the mean strain rate in the ϵ equation (25), which is introduced from the contraction of the anisotropic dissipation rate tensor transport equation.

Figure 3 shows the prediction patterns of both the streamwise velocity contour and the secondary flow in the x-y cross-section of the non-rotating square duct for the present model, Thielen-EBM and LES of Pallares and Davidson[7]. The secondary flow pattern and streamwise velocity component contour are reproduced well by the present model rather than the Thielen-EBM when they are compared to the LES. It is noted that the streamwise mean velocity, W, is rescaled with dividing it by u_τ. The position of the vortex core is in reasonable agreement with the LES. The predominant effect of the secondary motion is the induced transport of streamwise momentum towards the corner region.

Figure 4 shows that the distributions of the secondary mean velocity by both models are compared to the DNS data of Gavrilakis[8], and the profiles due to the present
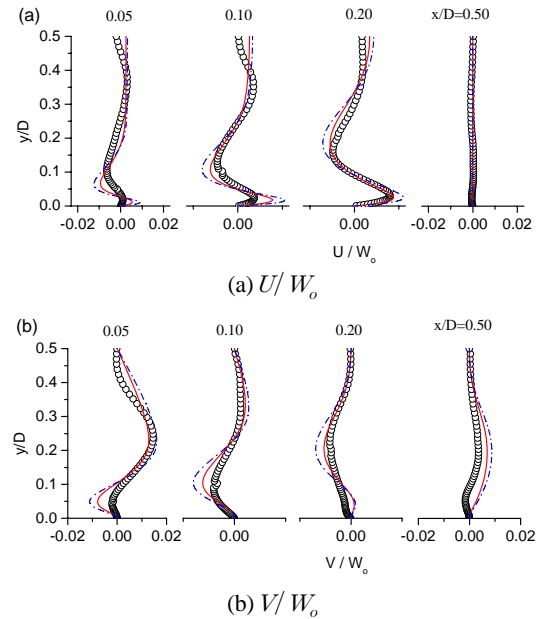

(a) U/W_o

(b) V/W_o

Figure 4 Secondary mean velocity distributions in a non-rotating square duct at $Re_\tau = 300$. (symbols: DNS of Gavrilakis[8]; —— : Present; —·— :Thielen-EBM).
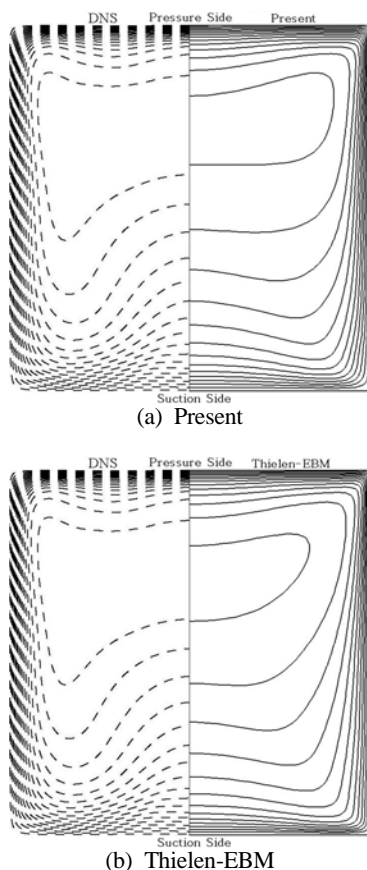
(a) Present

(b) Thielen-EBM

Figure 5 Contours of streamwise mean velocity in a rotating square duct for $Re_\tau = 300$ and $Ro_\tau = 0.38$.

model are predicted better than those of the Thielen-EBM. From this calculation, we can see that the prediction of secondary flow in a square duct is improved and affected by the present amended ADRM.

Figure 5 shows that the contours of the streamwise mean velocity for $Re_\tau = 300$ and $Ro_\tau = 0.38$ are compared to the DNS data of Gavrilakis[8]. Although some discrepancies exist in the pattern of the model predictions, the distortion shape caused by the rotation is similar to that of the DNS. This figure also shows the general effects of the mean streamwise velocity component distribution on the rotation effect. That is, as shown in this figure, the Coriolis effect causes the contour of the main velocity to bulge toward the corners and to shift the position of the maximum wall shear stress away from the center planes.

5. CONCLUSIONS

Concerning the predictions for the non-rotating channel, which is used for the decision of model coefficients appearing in the amended ADRM, the distributions of the mean velocity and the Reynolds stress due to the present model are more appropriately reproduced than those of the Thielen-EBM. Also, the decided coefficients

show the validity on the test for inhomogeneous shear flow in a rotating frame.

One the other hand, the under-estimated Reynolds stress distributions are reproduced on the suction side for higher rotation rates; however, the prediction results for the rotating channel flow due to the present model are captured reasonably well at relatively lower rotation rates. Therefore, prior to the application of the present model for rotation devices, we think that the problem of rapid relaminarization induced from increasing rotation rates must be resolved from the complement of the present model.

Although some discrepancies exist in the non-rotating square duct flow prediction, the secondary flow distributions are predicted reasonably well by the present model. Also, it can be seen that the streamwise mean velocity contour predictions due to the present model are closer to the DNS for rotating square duct flows than those of the Thielen-EBM.

Finally, the overall results that we presented are in reasonable agreement with the DNS and LES data, which provides confidence that the present elliptic-blending second-moment closure, which is based on the amended ADRM, can be applied to various industrial flows.

REFERENCES

[1] Speziale CG, Gatski TB. Analysis and modelling of anisotropies in the dissipation rate of turbulence. J. Fluid Mech. 1997;344:155-80.

[2] Mashayek F, Taulbee DB. Turbulent gas-solid flows, part II: explicit algebraic models. Numerical Heat Transfer B 2002; 41:31-52.

[3] Thielen L, Hanjalic K, Jonker H, Manceau R. Prediction of flow and heat transfer in multiple impinging jets with an elliptic-blending second-moment closure. Int. J. Heat Mass Transfer 2004;48:1583-98.

[4] Rogers MM, Moin P, Reynolds W C. The structure and modeling of the hydro dynamic and passive scalar fields inhomogeneous turbulent shear flow. Stanford University Tech. Rep., TF-25, 1986.

[5] Moser RD, Kim J, Mansour NN. Direct numerical simulation of turbulent channel flow up to $Re_\tau = 590$. Phys. Fluids 1999;11:943-5.

[6] Durbin PA. A Reynolds stress model for near-wall turbulence. J. Fluid Mech. 1993;249:465-98.

[7] Pallares J, Davidson L. Large-eddy simulation of turbulent heat transfer in stationary and rotating square ducts. Phys. Fluids 2002;14:2804-16.

[8] Gavrilakis S. private communication.